

Shear Capacity Analysis of Steel Reinforced Lightweight Concrete Elements Based on The Bond Strength

Jianwen ZHANG*, Yin ZHANG, Chen GAO, & Mengke SHI

College of Civil Engineering, Henan University of Engineering, Zhengzhou, China

*E-mail: hnnyzjw@126.com

ABSTRACT: Push-out tests of steel reinforced lightweight concrete (SRLC) were carried out for nine specimens which were designed according to the orthogonal test method considering four influence factors including strength of lightweight aggregate concrete, stirrup ratio, thickness of protective layer and anchorage length. The curves of average bond stress and loading-end slip were drawn, the characteristics of split failure and push-out failure were analyzed, and the characteristic bond strength was obtained. Combined with the test results of other scholars on the ultimate bond strength of steel reinforced concrete (SRC), it is found that the bond strength of SRLC is not worse than that of normal concrete (NC) which can be taken the same as 0.5MPa. Then the obtained bond strength can be used to calculate the shear strength of SRLC elements which may occur two forms of shear failure-diagonal shear failure and shear bond failure, however, shear bond failure is ignored in some specifications. Shear bond failure capacity computational formula of SRLC elements is deduced into which the bond strength is introduced. To verify the reasonability and accuracy of the proposed approach, the shear capacity and failure pattern are predicted by the proposed means with previous test results and are also compared with other provisions. The analyses and calculations indicate that the proposed method can accurately predict the shear failure mode and the calculated shear capacity values are in better agreement with the experimental results.

KEYWORDS: Push-out Test; Bond Strength; Steel Reinforced Lightweight Concrete; Shear Failure.

1 INTRODUCTION

With the people's increasing requirements for large space and good performances for buildings, more and more new building materials and novel structural forms have been applied in the field of civil engineering. The apparent density of lightweight concrete (LC) is less than 1950 Kg/m^3 , which is lighter than NC. Light coarse aggregate comes from artificial manufacture, nature or industrial slag. SRLC combines the advantages of SRC and LC, so SRLC structure has the advantages as light weight, high strength, thermal insulation, environment protection and good seismic performance. It is suitable for high-rise and long-span buildings, which attracts a growing number of scholars to conduct more extensive studies on material and structural performance (WANG, and HAN et al, 2017; LIU and FAN et al, 2019; ZHEN and HU et al, 2015; HASSANPOUR and SHAFIGH et al, 2014; HE and ZHANG et al, 2022).

The shear properties of SRLC (LIU and WANG et al, 2009; JIN, 2008; ZHU and SHAO, 2021) and SRC members (YANG and YU et al, 2017; BAI and JIANG, 2018) have been experimentally studied in which the shear span ratio ranges from 1 to 3. The above tests' results show that the shear properties and failure modes of SRLC and SRC members are similar, and there are two possible failure modes (WENG

and YEN et al, 2001) diagonal shear failure and shear bond failure. The diagonal shear failure is similar to that of ordinary reinforced concrete (RC) members. When the steel flange width is large approaching the overall section, the shear bond failure can be critical, which results in cracks along the interface of the steel flange and concrete. Japanese AIJ-SRC specification (AIJ, 1998) uses the superposition principle to calculate the shear strength of composite components. Although shear bond failure is considered in the calculation of bearing capacity in The Japanese code, the bond strength between section steel and concrete is not reflected in the formula. ACI specification (ACI, 2011) does not specify the difference between shear bond failure and diagonal shear failure but stipulated the calculation formula of RC members' bearing capacity. In NEHRP seismic code (BSSC, 1997) of the United States, the shear strength of concrete is ignored and only the shear strength of section steel web and stirrup is calculated. In Chinese Technical Specification for Steel Reinforced Concrete Composite Structures (JGJ138, 2016) the superposition method is adopted to calculate the contribution of concrete, stirrup, and sectional steel webs respectively. The shear span ratio is taken into account in the calculation formula, but the possible shear bond failure is not considered. Studies in literature (BAI and JIANG, 2018) indicate that calculation would be unsafe without considering shear bond failure which can be easy to happen under repeated loads.

The bond strength between concrete and steel is the main factor affecting the bearing capacity and deformation performance of SRLC members and is also an important parameter in structural finite element analysis. The experimental study (NAWAZ and ABDALLA et al, 2019) on the shear capacity of lava lightweight aggregate concrete beams showed that LC revealed better bonding performance than LC due to the shrinkage of aggregate. The experimental study on CFST bond performance in literature (NATALY and XAVIER et al, 2021) indicated that the bond strength between LC (coarse aggregate is ceramsite) and steel is higher than that of NC. The research on the bond performance of EPS LC (PECCE and CERONI, 2015) showed that the bond strength of EPS LC can be observed to increase significantly compared with NC at the same concrete strength level. Regardless of whether the coarse aggregate is lava or ceramsite and EPS, the bond strength of LC is higher than that of NC. On the above accounts, bond strength can't be ignored in the calculation of bearing capacity of SRLC elements. Therefore, the shear capacity formula of SRLC can be established with referenc to that of SRC, in which shear bond failure mode and bond strength should be reasonable considered for providing more scientific basis and safety guarantee for engineering design.

2 TEST PROGRAM

2.1 Specimen design

Nine push-out specimens were designed by orthogonal method considering four factors of concrete strength f_{cu} , anchorage length l_a , thickness of concrete protective cover C and stirrup reinforcement ratio ρ_{sv} with three levels for each factor, as can be seen in Table 1 in which b and h represent the section width and height of the specimen.

Table 1. Description of push-out specimens

NO.	$b \times h$ (mm)	f_{cu} (MPa)	l_a (mm)	C (mm)	ρ_{sv} (%)
L1	200×200	LC20	200	50	0.5
L2	250×250	LC20	400	75.5	0.2
L3	300×300	LC20	800	100	0
L4	250×250	LC25	200	75.5	0
L5	300×300	LC25	400	100	0.335
L6	200×200	LC25	800	50	0.25
L7	300×300	LC30	200	100	0.17
L8	200×200	LC30	400	50	0
L9	250×250	LC30	800	75.5	0.4

2.2 Materials

LC20, LC25 and LC30 grade light aggregate concrete were used in specimens. Coarse aggregate

adopted round spherical clay ceramsite of 700 grades with apparent density 1300 Kg/m^3 . Fine aggregate was river sand, and the actual sand rate was 38%. Portland cement type 42.5R was used. The mix proportions of the LC are given in Table 2 in which ρ_d represents dry apparent density.

Table 2. Mix proportion of concrete

Concrete strength	Dosage/ $\text{Kg} \cdot \text{m}^{-3}$				
	Cement	Ceramsite	Sand	water	ρ_d
LC20	400	533	653	263	1646
LC25	450	520	637	262	1675
LC30	490	510	624	261	1698

Water consumption in table 1 refers to the total water consumption after considering additional water consumption (WANG and LIU, 2006) for water absorption rate of ceramsite is 10%. Concrete cubic compressive strength f_{cu} , splitting tensile strength f_t , and elastic modulus E are shown in Table 3.

Table 3. Mechanics performances of LC

Concrete strength	f_{cu} (MPa)	f_t (MPa)	E ($\times 10^4 \text{MPa}$)
LC20	24.2	2.237	1.863
LC25	25.3	2.666	1.916
LC30	30	2.895	1.954

Table 4 lists yield strength f_y , ultimate strength f_u and ultimate elongation δ_u of the section steel, longitudinal reinforcement, and stirrup. The section steel adopts I10.

Table 4. Physical properties of steel

Steel category	f_y (MPa)	F_u (MPa)	δ_u
Section steel	315	418.7	23%
Longitudinal reinforcement	370	571	20%
Stirrup	336	489.3	19%

2.3 Loading test scheme

The push-out test program was carried out by a 500t compression testing machine in the Testing Center of College of Civil Engineering in Southeast University. Each step load is 10% of the predicted failure load before cracking and each load is 5% after cracking until to specimen destroyed. Before real loading 5~15kN should be preloaded first to ensure that there will be no load loss caused by initial settlement. The topside of section steel attaches to the compression testing machine with a complete steel plate. The hole at the free end of the specimen is reserved 50mm high, and the local compression part is embedded on a 10mm thick steel plate. The test device is shown in figure 1. The data will be read after 5 minutes of each stage loading.

3 TEST RESULTS AND ANALYSIS

3.1 Failure mode

Split failure occurred for specimens of L1, L2, L3, L4, L7 and L8, and push-out failure occurred for other specimens. Figure 4 shows failure photos of specimens.



Figure 1. Test setup



(a) Split failure



(b) Push-out failure

Figure 4. Specimen failure photos

2.4 Measurement method

Strain gauges on section steel and concrete are shown in figure 2 and figure 3 respectively. Strain gauges were arranged on the inner and outer side of section steel flange and the web. The position of concrete strain gauge corresponds to section steel with a 100mm spacing. In order to avoid the singularity of bond stress at the loading end, a non-bond area of 200 mm was set at the loading end. Two dial indicators are arranged at the loading end and the free end of the specimen respectively to measure the slip relative to the section steel. The specimens were cast with section steel in a horizontal position.

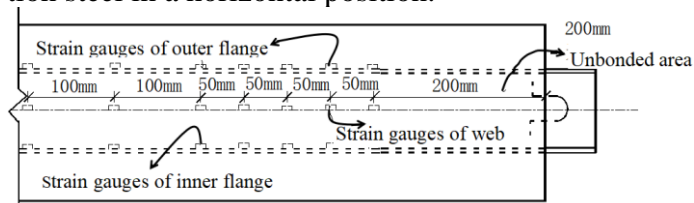


Figure 2. Section steel strain gauge arrangement

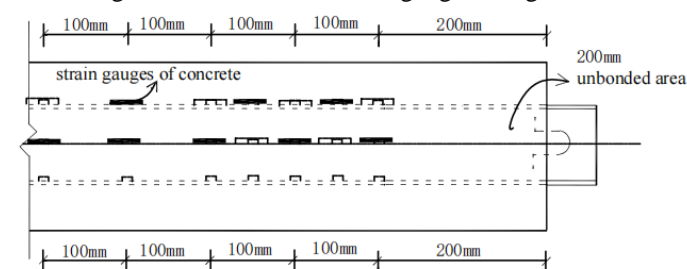


Figure 3. Concrete strain gauge arrangement

When the stirrup configuration is less, the anchorage length is shorter or the protective layer is thinner, the splitting failure occurs. When the load is increased to 10% ~ 35% of the ultimate load for the split failure specimen, fine cracks and slippage begin to appear at the loading end. There are three cracks' forms as shown in Figure 5. When the load exceeds 80% of the ultimate load, the slip growth rate accelerates. When it reaches the ultimate load, the load drops sharply, and the slip increases greatly with a loud sound of "bang". One or two of the original fine cracks suddenly go through the whole specimen, concrete was cracked, and the maximum crack width can reach 5 mm. The appearance and development of cracks in the specimens with stirrups are slower than those without stirrups, and the width of cracks is significantly narrower than that of the specimens without stirrups.

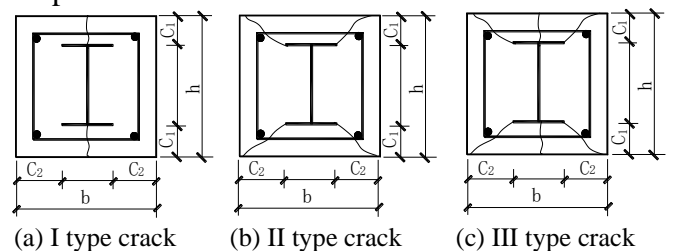


Figure 5. Crack type of the loading end

Push-out failure occurs when the stirrup configuration is dense, the anchorage length is long, or the protective layer is thick. When the load is small

(about 10% ~ 35% of the ultimate load), no slip occurs in the specimen. With the increase of load, the slip increases almost linearly in proportion to the load. When the load is about 60% ~ 80% of the ultimate load, there are thin cracks at the loading end of the specimen, and the cracks are of type II and III. When the ultimate load is reached, the load remains unchanged while the slip continues to increase and tends to be non-convergent. Cracks develop slowly and there are almost no cracks in the column or only some tiny cracks near the loading end.

3.2 Load-slip curves

Figure 6 shows the relationship curves of load P and loading end slip S_L

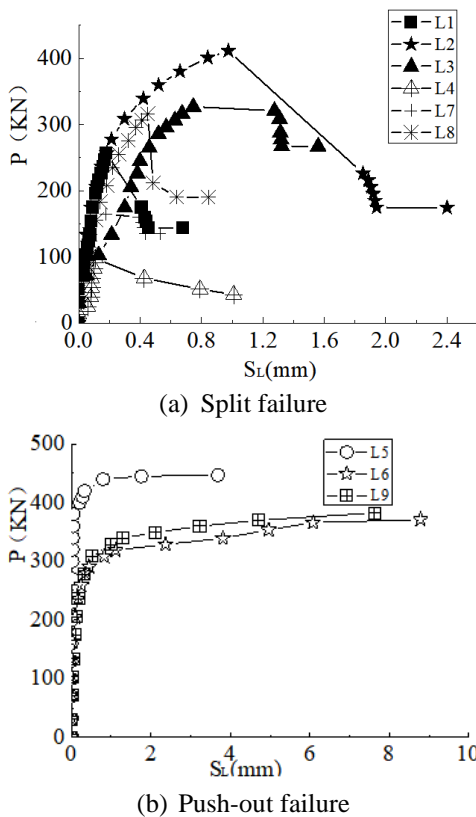


Figure 6. P- S_L measured curves

The load increases step by step according to 10% of the predicted failure load at each level of loading before cracking and 5% of the predicted failure load at each level of loading after cracking until the ultimate load is reached. The slip was read and recorded 5 minutes after each level of load was held. Synchronous slip is recorded with the load data by artificial reading.

When the ultimate load is reached for the splitting failure specimen, the load drops suddenly, and the slip increases rapidly until the residual load stage where the load remains relatively stable. The load slip curve of the specimen with split failure has an obvious descending section. As the load drops rapidly, less data can be read simultaneously in the falling section. When the load is relatively stable, some data can

be read. When the ultimate load is reached, the load remains unchanged and the slip increases for push-out failure specimens.

According to the analysis of the above measured curves, P- S_L relationship model is established as shown in Figure 7.

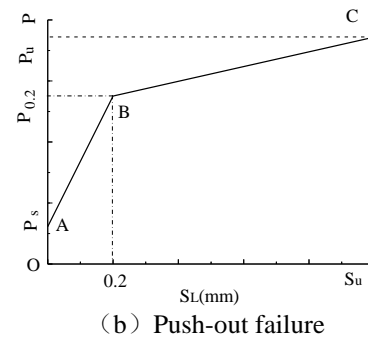
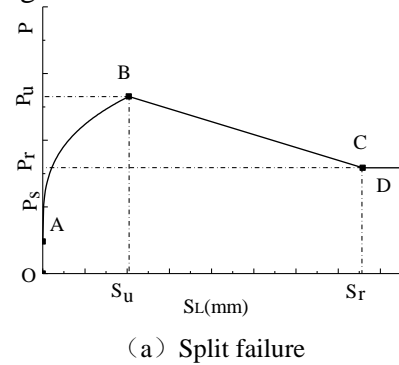


Figure 7. P- S_L relationship model

When the stirrup ratio is less, the anchorage length is shorter or the protective layer is thinner, the splitting failure occurs. The load-slip curve of split failure specimens can be divided into four sections: non-slip section, rising section, falling section and residual section. The chemical cementing force in the non-slip section plays a major role. As the load increases, the loading end starts to slip accompanied by the decrease of chemical cementation force when the corresponding load reaches the initial slip load P_s . Subsequently friction force and mechanical bite force begin to play a role until the ultimate load P_u . At ultimate load due to the lack of effective restraint of concrete, it causes the concrete splitting for friction and mechanical bite force is not enough to resist the interface shear force. After the splitting failure occurs, the friction force disappears, and the mechanical bite force plays a contributing role. The end point of the decline segment is the starting point of the residual segment, and the load is denoted as P_r . The slip corresponding to ultimate load P_u and residual load P_r are ultimate load slip S_u and residual slip S_r respectively.

Push-out failure occurs when the stirrup configuration is dense, the anchorage length is long, or the protective layer is thick. The load-slip curve of the specimen can be divided into three sections: non-slip section, rising section and big slip section. The bonding mechanism of non-slip section and rising section is the same as that of splitting failure. When the slip at the loading end is up to about 0.2mm, the curve

presents an obvious turning point and begins to enter the stage of major slip. The turning point load is denoted as $P_{0.2}$. Following the rising section because the concrete is better restrained causing greater friction and mechanical bite force on the steel and concrete interface, the bearing capacity of the specimen can continue to grow while enduring significant slippage until to ultimate load P_u . The slip corresponding to ultimate load P_u is ultimate load slip S_u .

3.3 Characteristic bond strength

Formula (1) gives the express of the average bond stress $\bar{\tau}$ which can be obtained by dividing the load P by the total surface area of section steel $L\Sigma o$ of the specimen with anchor length L and the total perimeter of section steel Σo .

$$\bar{\tau} = P / L\Sigma o \quad (1)$$

The characteristic bond strength reflects the average bond stress on the contact surface when the characteristic load is reached. Three characteristic loads of splitting failure are the initial slip load P_s , ultimate load P_u and residual load P_r , and the corresponding characteristic bond strength is initial slip bond strength $\bar{\tau}_s$, ultimate bond strength $\bar{\tau}_u$ and residual bond strength $\bar{\tau}_r$ respectively. It is deduced that push-out failure has the same characteristic bond strength $\bar{\tau}_s$ and $\bar{\tau}_u$. According to the load-slip curve of push-out failure specimens derived, when the load reaches to $P_{0.2}$, then the corresponding characteristic bond strength is the turning point bond strength denoted as $\bar{\tau}_{0.2}$. The characteristic bond strength of the specimens is listed in Table 5.

After the test, some residual concrete debris on the surface of the section steel was found when the specimen was broken open and no honeycomb or cavity was found under the specimen indicating that the casting quality of the specimen was good.

Table 5. Characteristic bond strength

NO.	$\bar{\tau}_s$ (MPa)	$\bar{\tau}_{0.2}$ (MPa)	$\bar{\tau}_r$ (MPa)	$\bar{\tau}_u$ (MPa)
L1	0.679	/	1.58	2.83
L2	0.283	/	0.962	2.264
L3	0.142	/	0.736	0.9
L4	0.2	/	0.476	1.076
L5	0.85	2.26	/	2.548
L6	0.34	0.68	/	1.022
L7	0.18	/	1.49	1.8
L8	0.623	/	1.047	1.738
L9	0.142	0.68	/	1.053

3.4 Ultimate bond strength

Ultimate bond strength $\bar{\tau}_u$ is the average bond stress under ultimate load P_u . Because the actual bond stress varies along the direction of anchorage length, this strength is generally used as the bond strength in engineering application.

The expression that the bond strength between steel plate and concrete is directly proportional to the compressive strength of concrete is given by literature (AIJ, 1998) from Japan as follows.

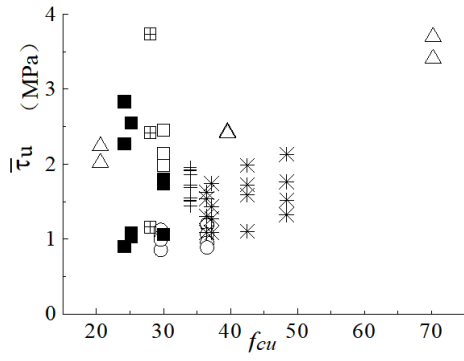
$$\bar{\tau}_u = 0.02f_c \quad (2)$$

Through statistical regression of Roeder's test results (ROEDER, and CHMIELOWSKI et al, 1999), Sun Guoliang (SUN and WANG, 1989) obtained a linear relationship formula for the average bond strength and concrete tensile strength of SRC on the flange edge, as shown in the following formula.

$$\bar{\tau}_u = 0.5644f_t \quad (3)$$

Eurocode 4 (EUROCODE NO.4, 2004) allows the use of natural bond strength of 0.5 MPa along the perimeter of the steel section within the anchorage length of the maximum section size, while the Japanese code allows the use of bond strength to be no more than 0.45 MPa (AIJ, 1998) along the whole anchorage length. Lu Chunyang (LU and WANG et al, 2007) learned from the tests that the bond of ceramsite concrete is greater than that of LC. Research (CHEN and ZENG et al, 2005) on ceramsite concrete showed that the bond stress of LC distributes more evenly along the anchorage length.

It can be seen from the above research results that the lower limit of bond strength given by different countries is different due to the variability of materials, different test methods and complexity of bond mechanism. Scatter diagram of the ultimate bond strength and concrete compressive strength is listed in figure 8 including the experimental results of Bryson (BRYSON and MATHEY, 1962), Liu Can (LIU and HE, 2002), Roeder (ROEDER, and CHMIELOWSKI et al, 1999), Shao Yongjian (SHAO, 2003), Yang Yong (YANG and GUO et al, 2005) Liu Kun (LIU and ZHANG, 2012) and this test. As can be seen from Figure 8, the bond strength of SRLC is not lower than that of SRC and the data is highly dispersed, but the lower limit of bond strength is more than 0.5 Mpa which can be adopted as the bond strength of SRLC and SRC.

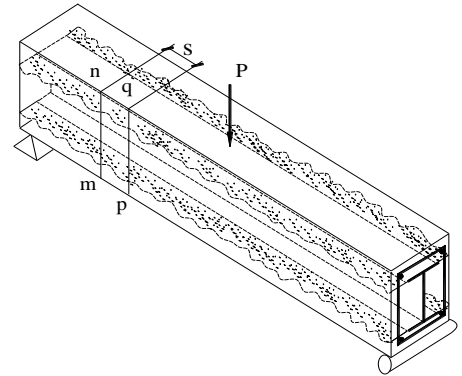


□ Bryson1962NC △ Liu2002NC ○ Roeder1999NC
+ Shao2003NC * Yang2005NC ⊞ Liu2012LC ■ This test LC
Figure 8. Scatter diagram bond strength

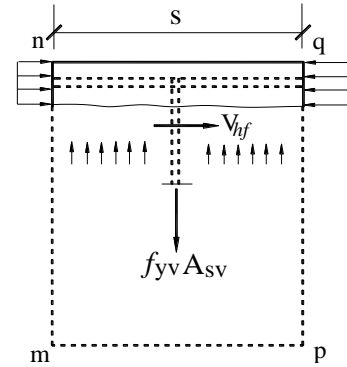
$$V_{rc1} = 0.8f_tbh_0 + \frac{f_{yv}A_{sv}h_0}{s} \quad (9)$$

4.3 Shear bond capacity of RC V_{rc2}

Figure 9(a) illustrates the shear bond cracks along the interface of steel flanges and concrete. Figure 8 (b) is the force diagram of the upper part of the interface crack within the stirrup spacing length which displays the horizontal shear force V_{hf} along the cracked plane.



(a) Interfacial cracks of shear bond failure



(b) Horizontal shear force V_{hf} along the cracked plane

Figure 9. Force diagram of shear bond failure

Horizontal shear force V_{hf} consists of two parts: one is the horizontal shear friction force named as V_{hf1} provided by the concrete part at the interface crack, the other part is the horizontal bond force denoted by V_{hf2} provided by the steel flange and concrete interface.

$$V_{hf} = V_{hf1} + V_{hf2} \quad (10)$$

Weng C C (WENG and YEN et al, 2001) provides the formula of horizontal shear force V_{hf} in which the contribution of the bond stress between the steel flange and concrete is negligible. According to literature (WENG and YEN et al, 2001), V_{hf1} is calculated as follows

$$V_{hf1} = \mu_f A_{sv} f_{yv} + K_1 A_{ch} \quad (11)$$

The first term represents the interface friction force, and the second term represents the pin bolt force and the bite force of the interface protrusion aggregate in formula (11). Where μ_f is friction coefficient which is taken as 0.8 when concrete slips relative to concrete; K_1 is empirical constant usually taken equal to 2.8 MPa; A_{ch} is area of concrete

4 SHEAR FAILURE MODEL

4.1 Prediction model

According to Code for Design of Composite Structures (JGJ138, 2016), the shear capacity of SRLC composite member V_u adopts the same composition mode as that of SRC member, which is composed of the shear capacity of reinforced concrete (RC) part V_{rc} and the shear capacity of section steel part V_{ss} . That is

$$V_u = V_{rc} + V_{ss} \quad (4)$$

However, shear bond failure is not considered in literature (JGJ138, 2016). The following will introduce how to consider the contribution of diagonal shear failure and shear bond failure in the calculation of concrete shear capacity.

$$V_{rc} = \min(V_{rc1}, V_{rc2}) \quad (5)$$

In the formula, V_{rc1} and V_{rc2} denote the diagonal shear capacity and shear bond capacity of concrete respectively. V_{rc} is determined as the smaller value of the V_{rc1} and V_{rc2} .

Under the concentrated load it is needed to consider the influence of shear-span ratio λ , so V_{ss} is expressed as the following formula.

$$V_{ss} = \frac{0.58}{\lambda} f_a t_w h_w \quad (1.5 \leq \lambda \leq 3) \quad (6)$$

Where f_a is the yield strength of section steel, t_w and h_w are the thickness and height of the flange web respectively.

Generally, V_{ss} is

$$V_{ss} = 0.58 f_a t_w h_w \quad (7)$$

4.2 Diagonal shear capacity of RC V_{rc1}

V_{rc1} caused by concentrate load is expressed as

$$V_{rc1} = \frac{1.75}{1+\lambda} f_t b h_0 + \frac{f_{yv} A_{sv} h_0}{s} + 0.07N \quad (1.5 \leq \lambda \leq 3) \quad (8)$$

Where f_t is the tensile strength of concrete; b and h_0 is the section width and effective height; f_{yv} , A_{sv} and s is the yield strength, area and space of the stirrup; N is axial load applied to the member.

Normally V_{rc1} can be expressed as

resisting the horizontal shear friction force within a distance s , taken as follows

$$A_{ch} = (b - b_f)s \quad (12)$$

Where b_f denotes to the width of the steel flange.

Formula (13) gives the calculation formula of horizontal shear bond force V_{hf2} .

$$V_{hf2} = \bar{\tau}_u b_f s \quad (13)$$

$\bar{\tau}_u$ is the interface bond strength between the section steel and concrete taken as 0.5 MPa according to the foregoing test analysis.

Substitute formulas (11), (12) and (13) into formula (10), and you get

$$\begin{aligned} V_{hf} &= V_{hf1} + V_{hf2} \\ &= \mu_f A_{sv} f_{yv} + K_1 (b - b_f) s + \bar{\tau}_u b_f s \end{aligned} \quad (14)$$

The maximum average horizontal shear stress τ_1 generated by horizontal shear force V_{hf} on cracked surface within stirrup spacing range s can be expressed as

$$\tau_1 = \frac{V_{hf}}{bs} \quad (15)$$

The shear stress τ_2 resulting from applied shear force V_{rc} of the RC portion at the location of the cracked surface can be calculated as follows:

$$\tau_2 = \frac{V_{rc} S_x}{I_x b_{be}} \quad (16)$$

Where S_x indicates the first moment of the concrete area above the interface about the neutral axis of the RC portion; I_x denotes moment of inertia of the RC portion; b_{be} represents the effective width of the concrete section to resist shear bond failure taken as $b - b_f$. Generally, the steel section ratio is about 5% for SRLC and SRC elements, so the effective width b_{be} is adopted as 95% of the section width b .

In order to simplify the calculation, the shear stress is assumed distributed uniformly on the effective area A_{cv} which is equal to be $0.95 b \times d$, then

$$\tau_2 = \frac{V_{rc}}{0.95bh} \quad (17)$$

Where h is the total depth of the member.

To avoid shear bond failure, τ_2 should not be larger than τ_1 . That is

$$\begin{aligned} \frac{V_{rc}}{0.95bh} &\leq \frac{V_{hf}}{bs} \\ V_{rc} &\leq \frac{0.95V_{hf}h}{s} \end{aligned} \quad (18)$$

Substituting (14) into (18) leads to

$$V_{rc} \leq 0.95[\mu_f A_{sv} f_{yv} h / s + K_1 (b - b_f) h + \bar{\tau}_u b_f h] \quad (19)$$

Equation (20) indicates that the shear bond capacity of RC can be expressed as

$$V_{rc2} = 0.95[\mu_f A_{sv} f_{yv} h / s + K_1 (b - b_f) h + \bar{\tau}_u b_f h] \quad (20)$$

4.4 Verification analysis

In order to verify the applicability of the above formula, a verification analysis is made between the test results which were conducted by Zhang et al (ZHANG and YAMADA, 1992) and the proposed approach. The specimen parameters are shown in Table 6. The concrete protection layer of all specimens in the table is 15mm thick with longitudinal deformed reinforcements 10 mm in diameter at the four corners. The cross section of the specimens is square with a side length 125 mm. The encased wide flange steel was built up by fillet welding from a steel plate 2 or 3.2 mm in thickness. Where d_s and t_f indicate the height and the flange thickness of the encased steel respectively. The stirrup is made by smooth round bars 3 mm in diameter with a spacing of 50mm. Where F_{ys} and F_{yh} denote the yield strength of the steel section and stirrup respectively; the axial force applied is named as N_u ; and V_{test} represents the shear test value of specimen.

Table 6. Specimen parameter

NO.	$d_s \times b_f \times t_w \times t_f$ (mm)	ρ_{sv} (%)	F_{ys} (MPa)	F_{yh} (MPa)	f_c (MPa)	N_u (KN)	V_{test} (KN)
1	H-80×80×2.0×2.0	0.23	254	297	43.9	294	52.7
2	H-80×60×2.0×2.0	0.23	270	297	32.6	121	57.1
3	H-80×60×2.0×2.0	0.23	270	297	28	217	57.1
4	H-80×60×2.0×2.0	0.23	270	297	31.6	483	55.9
5	H-50×60×3.2×3.2	0.23	290	297	32.8	223	54.9

The comparison between the test results and the prediction of the proposed approach、AIJ-SRC code and the algorithm in literature (WENG and YEN et al, 2001) are shown in Table 7. Where V_{AIJ} 、 V_{prod} and $V_{[11]}$ stand for the shear strength predicted by AIJ-SRC code、proposed approach and literature (WENG and YEN et al, 2001) respectively; SB and DS represent shear bond failure and diagonal shear failure individually.

The analyses in Table 7 show that the average ratio of the shear capacity calculated by AIJ-SRC code to the test results is 0.921 with a standard deviation of 0.037, indicating that the bearing capacity is in good agreement with the test results. However, the predicted failure modes are quite different from the experimental results. Except specimen NO.1 was shear bond failure, the others were diagonal shear failure. This is mainly because the axial force is not considered in the calculation formula of shear capacity for AIJ-SRC code. The bond between the steel section and concrete is not considered both in AIJ-SRC code and in reference (WENG and YEN et al, 2001). The average ratio of the predicted value to the test result is 0.938 with a standard deviation of 0.05 for literature (WENG and YEN et al, 2001), and 0.96 with a standard deviation of 0.036 for the proposed approach. It is observed that the proposed approach can

simulate failure mode more reasonably and predict bearing capacity more accurately.

Table 7. Shear capacity comparison between the calculated values and the test results

NO.	V_{test} (KN)	V_{AIJ} (KN)	$V_{[11]}$ (KN)	V_{prod} (KN)	V_{AIJ} / V_{test}	$V_{[11]}$ / V_{test}	V_{prod} / V_{test}
1	52.7SB	49.8SB	45.6SB	48.1SB	0.945	0.865	0.91
2	57.1SB	51.3DS	53.3SB	54.2SB	0.898	0.933	0.95
3	57.1SB	50.1DS	53.3SB	54.2SB	0.877	0.933	0.95
4	55.9SB	51.1DS	53.3SB	54.2SB	0.914	0.953	0.97
5	54.9SB	53.2DS	55.2SB	56SB	0.969	1.005	1.02
Average ratio:					0.921	0.938	0.96
Standard deviation:					0.037	0.050	0.036

To verify the validity of the prediction, model some SRC (JIN, 2008) and SRLC (ZENG and WANG et al, 2005) specimens are selected as shown in Table8. L1, L2 and L3 are SRLC specimens, the rest are SRC specimens. The cross-section size of SRLC specimen is 200 mm wide and 300 mm high, and the cross-section size of SRC specimen is 300 mm square. When the shear span ratio λ is between 1.5 and 2.5, shear bond failure occurred in these specimens. The experimental results are compared with the proposed calculation method. The calculation results show that the bearing capacity of SRC and SRLC members with shear bond failure is in good agreement with the experimental results. Specimens 3 and 4 have the same conditions except concrete strength. Shear bond failure occurred in both specimens and the calculated bearing capacity is the same. The experimental results show that the change of concrete strength has little effect on shear bond failure capacity. The situation of specimens 5 and 6 is the same as above.

Table 8. Comparison of specimens and calculation results

NO.	$d_s \times b_f \times t_w$ (mm)	λ	ρ_{sv} (%)	f_a (MPa)	f_{yv} (MPa)	V_{test} (KN)	V_{prod} (KN)	V_{prod} / V_{test}
L1	120×74×5.0	2.0	0.25	235	238	176.78	172	0.97
L2	120×74×5.0	2.5	0.25	235	238	160.65	165	1.027
L3	140×80×5.5	1.5	0.25	235	238	178.71	195	1.09
1	200×100×8	1.5	0.106	311	299	383.8	372.7	0.97
2	200×100×8	2.5	0.106	311	295	292	301	1.03
3	200×100×10	1.5	0.106	313	299	416.4	413.7	0.99
4	200×100×10	1.5	0.106	313	299	404.8	413.7	1.02
5	200×100×6	1.5	0.106	330	299	342	340	0.99
6	200×100×6	1.5	0.106	330	299	330.3	340	1.03

5 CONCLUSIONS

A push-out test was carried out for the bond performance of nine SRLC specimens. There happened two failure modes that were splitting failure and push-out failure and the experimental curves of load-slip were obtained. According to the test curves, the

failure characteristics of the two types of failure are analyzed and the characteristic values of bond strength are given.

The average bond strength of SRC and SRLC under ultimate load is analyzed and compared. It is found that the bond strength between the steel section and LC is not lower than that of NC, and the same value can be taken in the calculation of the composite member. Generally, 0.5 MPa is feasible.

The proposed approach of shear bearing capacity for SRLC members is more perfect because the shear bond failure that may occur is considered in which the bond strength is introduced. A verification between the test results and the calculated values for the proposed approach and other methods mentioned in this study was made, and the comparison results show that the proposed approach can not only satisfactorily estimate the shear failure model, but also accurately predicts the shear bearing capacity.

The calculation formula of shear bond failure capacity shows that the shear bond failure capacity decreases sharply with the increase of flange width and the composite members are more prone to shear bond failure. If the possible shear bond failure is not considered, the calculation results are unreliable (BAI and JIANG, 2018) and the shear bond failure capacity is less than the diagonal shear failure capacity in this case. The research aims to come up with a calculation formula of shear strength of SRC and SRLC members considering shear bond failure in which the bond strength between section steel and concrete is 0.5MPa. When the shear bond failure capacity is lower than the diagonal shear failure capacity, shear bond failure occurs in composite members and the shear bond failure capacity is calculated according to the proposed shear bond failure capacity formula. At present, there is few test data, especially for specimens with large cross-section size and high steel content of the section steel. Therefore, more tests are needed to study the shear bond failure performance of SRC and SRLC components, so as to further clarify the occurrence conditions and measures to be taken.

REFERENCES

- American Concrete Institute (ACI) Building code requirements for structural concrete (ACI 318-11). American Concrete Institute, Detroit, 2011.
- Architectural Institute of Japan (AIJ). Calculation Standard and Interpretation of Steel reinforced concrete Structures. Translated by Feng Naiqian, Ye Liping et al. Beijing: Energy Press,1998.
- Bai L G, Jiang W S. Discussion on shear bearing capacity of steel reinforced concrete members. Industrial Construction. 48 Supplement, 2018, PP 546-552.

- Bryson J O, Mathey R G. Surface condition effect on bond strength of steel beams in concrete. *Journal of ACI*, 59(3), 1962, PP 397-406.
- BSSC. NEHRP Recommended provisions for the development of seismic regulations for new buildings and other structures. Washington, D.C. 1997.
- Chen Y S, Zeng S H, Dong F Z et al. Experimental research on the bond stress distribution of deformed reinforcement in the lightweight reinforcement concrete. *Journal of Hubei University of Technology*. 20(2), 2005, PP 4-7.
- Code for Design of Composite Structures (JGJ138-2016). Beijing: China Building Industry Press, 2016.
- Eurocode No.4 Design of composite steel and concrete structures. Part 1: General rules for buildings. Commission of European Communities, Luxembourg, 2004.
- Hassanpour M, Shafiq P, Mahmud H. Mechanical properties of structural lightweight aggregate concrete containing low volume steel fiber. *Arabian Journal for Science and Engineering*. 39, 2014, pp 3579-3590.
- He Y C, Zhang H J, Wang J F, Liu W, Liu Y. Investigation on axial compressive behavior of partially-encased composite steel and lightweight aggregate concrete long columns. Progress in steel building structures. <https://kns.cnki.net/kcm/detail/31.1893.TU.20220314.1628.008.html>.
- Jin H. Study on shear capacity of steel - reinforced lightweight aggregate concrete. *Science and Technology Innovation Herald*. 30, 2008, pp 26.
- Liu C, Fan Z Y, Chen X N, Zhu C, Wang H, Bai G L. Experimental study on bond behavior between section steel and RAC under full replacement ratio. *Journal of civil engineering*. 23 (3), 2019, PP 1159-1170.
- Liu C, He Y B. Experimental study on bond behavior of steel reinforced concrete. *Journal of Hunan University (Natural Sciences Edition)*. 29(3), 2002, pp 168-173.
- Liu F, Wang X H, Shao Y J, Zhao H T, Xia M. Experiment and calculation of shear capacity of steel reinforced lightweight aggregate concrete beams. *Building Structure*, 39 (6), 2009, PP 9-21.
- Liu K, Zhang T T. Experimental study on bonded behavior of steel reinforced lightweight concrete. *Steel construction*, 27 (8), 2012, pp 1-5.
- Lu C Y, Wang W Y, Li P N. Experiment research on bond behavior between deformed bar and lightweight concrete. *Journal of Guangxi University*. 32(1), 2007, PP 6-9.
- Natalli J F, Xavier E M, Costa L C B et al. New methodology to analyze the steel-concrete bond in CFST filled with lightweight and conventional concrete. *Materials and Structures*. 54, 2021, pp 1-13.
- Nawaz W, Abdalla J A, Hawileh R A et al. Experimental study on the shear strength of reinforced concrete beams cast with lava lightweight aggregates. *Archives of Civil and Mechanical Engineering*. 19, 2019, pp 981-996.
- Pecce M, Ceroni F. Steel-concrete bond behaviour of lightweight concrete with expanded polystyrene (EPS). *Materials and Structures*. 48, 2015, pp 139-152.
- Roeder C W, Chmielowski R, Brown C B. Shear connector requirements for embedded steel sections. *Journal of Structural Engineering*. 125, 1999, pp 142-151.
- Shao Y J. Study on bond behavior of steel reinforced concrete structure. *China Cement and Concrete Products*. 132, 2003, PP 23-25.
- Sun G L, Wang Y j. Experimental study and calculation of axial load transmission in the top section of encased columns. *Journal of structures*. 6, 1989, PP 40-49.
- Wang J J, Liu Z Q. The characters and developments of new light weight aggregate concrete. *Concrete*. 2006, pp 65-66.
- Wang W H, Han L H, Tan Q H, Tao Z. Test on the steel-concrete bond strength in steel reinforced concrete (SRC) columns after fire exposure. *Fire Technology*. 53, 2017, PP 917-945.
- Weng C C, Yen S I, Chen C C. Shear strength of concrete-encased composite structural members [J]. *Journal of Structural Engineering*, 127(10), 2001, pp 1190-1197.
- Yang Y, Guo Z X, Xue J Y et al. Experiment study on bond slip behavior between section steel and concrete in SRC structures. *Journal of Building Structures*. 26 (4), 2005, pp 1-9.
- Yang Y, Yu Y L, Yang Y, Shao Y J, Guo Y X, Xue J Y. Experimental study on shear performance of partially precast steel reinforced concrete beams. *Journal of Building Structures*, 38(6), 2017, PP 53-60.
- Zeng J M, Wang T C, Jiang W S. Analysis on shear strength of SRC column with bonding failure. *Journal of Harbin Institute of Technology*, 37, 2005, PP 532-534.
- Zhang F, Yamada M. Composite columns subjected to bending and shear. *Composite construction in steel and concrete II*, New York: ASCE, 1992, 483-498.
- Zhen H, Hu X M, Liu J R, Hong W. Experimental study on bond slip behavior between section steel and concrete in partially encased composite members. *Industrial Construction*. 45 (12), 2015, PP 183-188.
- Zhu P F, Shao Y J. Experiment and calculation of shear performance of steel reinforced lightweight aggregate concrete beams. *Journal of Suzhou University of Science and Technology (Engineering and Technology)*, 34 (3), 2021, PP 43-49.